Published by Avanti Publishers

International Journal of Architectural Engineering Technology

ISSN (online): 2409-9821

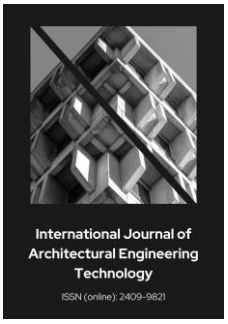

A Deep-Learning based Monthly Precipitation Forecasting with Implications for Urban Design and Water Management

Mohammad R.M. Behbahani[1,*] and Javad Teymoori[2]

[1]*Department of Civil and Environmental Engineering, University of Connecticut, Storrs, USA*

[2]*Department of Civil Engineering, University of Texas at Arlington, Texas, USA*

ARTICLE INFO

Article Type: Research Article

Academic Editor: Wenjian Pan

Keywords:
Deep learning,
Precipitation forecasting,
Urban water management,
Climate-responsive design,
Entropy-based wavelet decomposition.

Timeline:
Received: November 01, 2025
Accepted: December 05, 2025
Published: December 13, 2025

Citation: Behbahani MRM, Teymoori J. A deep-learning based monthly precipitation forecasting with implications for urban design and water management. Int J Archit Eng Technol. 2025; 12: 238-254.

DOI: https://doi.org/10.15377/2409-9821.2025.12.15

ABSTRACT

Accurate precipitation forecasting is essential for disaster preparedness and climate-responsive urban planning such as drainage designing under increasing climatic variability. This study investigates an entropy-guided deep learning framework to improve monthly precipitation forecasting by integrating the Maximal Overlap Discrete Wavelet Entropy Transform (MODWET) with a Gated Recurrent Unit (GRU) model. Unlike the conventional Maximal Overlap Discrete Wavelet Transform (MODWT), MODWET employs entropy to objectively determine the optimal wavelet filter and decomposition level, addressing a key limitation in wavelet-based preprocessing related to over- or under-decomposition of hydroclimatic signals. While the effectiveness of MODWET has previously been demonstrated for streamflow forecasting, its application to precipitation prediction has not yet been explored. The proposed framework is evaluated using monthly precipitation data from three hydrometeorological case studies close to urbane are, selected from the CAMELS dataset across the United States. Model performance is assessed using multiple statistical metrics, including NSE, RMSE, percent bias (PBIAS), and correlation coefficient (r^2). In addition, the Partial Correlation Index (PCI) is employed to identify informative predictors and reduce input redundancy. Results show that the hybrid PCI–MODWET–GRU model consistently outperforms the standalone GRU model, achieving improved correlation (up to $r^2 = 0.78$ at selected stations) and overall predictive accuracy. These findings highlight the potential of combining entropy-based wavelet preprocessing with deep learning models to enhance precipitation forecasting reliability, with direct relevance for urban and peri-urban water management and climate-responsive design applications. By improving the representation of seasonal and nonstationary precipitation behavior at monthly timescales, the proposed framework provides more stable and interpretable forecasts that can support early-stage urban planning, water-sensitive architectural design, and long-term infrastructure resilience assessments under evolving climate conditions.

*Corresponding Author
Email: mohammad_reza.mazarei_behbahani@uconn.edu
Tel: +(01) 860-634-8328

1. Introduction

Rapid urbanization, climate variability, and the increasing frequency of extreme precipitation events have placed unprecedented pressure on urban water systems and infrastructure [1]. Cities are particularly vulnerable to rainfall uncertainty due to high impervious surface coverage, limited infiltration capacity, aging drainage networks, and growing exposure to flood and waterlogging hazards [2]. As a result, accurate precipitation forecasting has become a critical component of urban water management, informing the design and operation of stormwater systems, flood mitigation strategies, reservoir regulation, and climate-resilient urban planning [3]. Reliable medium- to long-term precipitation predictions enable urban decision-makers to shift from reactive responses toward proactive and adaptive management of water-related risks [4, 5].

Beyond hydrological risk mitigation, precipitation patterns fundamentally shape the form, performance, and resilience of the built environment at multiple spatial scales [6-10]. In urban and architectural design, rainfall characteristics influence decisions related to building orientation, roof geometry, façade detailing, surface grading, and the allocation of open and permeable spaces within developments [11-13]. At the neighborhood and city scale, precipitation variability affects land-use planning, street layout, drainage corridors, and the integration of blue–green infrastructure aimed at managing runoff and enhancing urban livability [14-18]. Consequently, reliable precipitation information is increasingly viewed not only as an operational input for water management but also as a critical design parameter for climate-responsive urban development, particularly under conditions of increasing climatic uncertainty.

Accurate precipitation prediction provides essential decision-support information across multiple layers of urban systems and infrastructure. At the planning level, medium- to long-term precipitation forecasts inform the design and sizing of stormwater drainage networks, detention and retention facilities, and green infrastructure by characterizing expected rainfall variability and extremes [19-21]. At the operational level, forecasted precipitation can be used to optimize reservoir releases, regulate urban flood control structures, and improve the timing of maintenance and emergency response actions [22, 23]. In addition, reliable precipitation forecasts support urban water supply management by aiding demand planning, drought preparedness, and conjunctive surface–groundwater use strategies. Under climate change and rapid urban expansion, integrating data-driven precipitation forecasting into urban decision-making frameworks enables cities to anticipate hydrologic stresses, reduce flood risk, and enhance the resilience and sustainability of urban water systems [24-26].

Despite significant advances in numerical weather prediction and physically based hydrological models, precipitation forecasting remains a challenging task due to the nonlinear, nonstationary, and multi-scale nature of rainfall processes—particularly at monthly timescales relevant to urban infrastructure planning and operational decision-making [27-29]. These challenges are further exacerbated in urban contexts, where precipitation signals are often noisy and influenced by localized climatic effects, including urban heat islands and land-use heterogeneity. As a result, data-driven approaches, especially machine learning and deep learning models, have gained increasing attention for precipitation forecasting and urban water applications [30, 31].

Deep learning models such as recurrent neural networks (RNNs), long short-term memory (LSTM), and gated recurrent units (GRU) have demonstrated strong capabilities in capturing complex temporal dependencies in hydroclimatic time series [32-35]. Among these, GRU networks offer computationally efficient architecture with fewer parameters than LSTM while retaining strong performance in sequence modeling, making them attractive for large-scale and operational forecasting applications [36-38]. However, the predictive skill of deep learning models is highly dependent on data quality, feature representation, and preprocessing strategies. Without effective preprocessing, deep learning models may struggle to extract meaningful information from precipitation records characterized by multi-frequency variability and noise [39, 40].

Wavelet-based signal decomposition techniques have emerged as powerful preprocessing tools for hydrological and climatological forecasting, as they enable simultaneous representation of temporal and frequency-domain information [41, 42]. Among these methods, the MODWT has been widely adopted due to its ability to preserve temporal alignment and handle nonstationary signals [43-45]. Nevertheless, a persistent

limitation of wavelet-based approaches lies in the subjective selection of decomposition levels and wavelet filters, which can lead to redundant information or loss of essential signal characteristics [46, 47].

To address this limitation, Mazarei Behbahani and Mazarei [47] recently proposed the MODWET, an entropy-guided preprocessing framework that objectively determines the optimal wavelet filter and decomposition level. By minimizing information entropy, MODWET prevents over-decomposition and enhances the representation of informative signal components [48, 49]. While the effectiveness of MODWET has been demonstrated for streamflow forecasting using traditional machine learning models, its potential for precipitation forecasting—particularly in combination with deep learning architectures—has not yet been systematically investigated.

In this study, we address this gap by integrating MODWET with a GRU deep learning model for monthly precipitation forecasting. In addition, PCI is employed as a feature selection method to reduce predictor redundancy and improve model parsimony [50]. The proposed PCI–MODWET–GRU framework is evaluated using three hydrometeorological case studies from the CAMELS dataset, representing diverse climatic conditions [51]. Although the case studies are not limited to urban catchments, the proposed framework is directly applicable to urban water systems, where accurate precipitation forecasts serve as critical inputs for stormwater modeling, flood risk assessment, and climate-resilient infrastructure planning.

By improving the reliability and interpretability of precipitation forecasts at planning-relevant timescales, this research contributes to the development of data-driven tools that support urban water management and sustainable city design under increasing climatic uncertainty.

2. Case Study

We selected three representative watersheds from the CAMELS dataset to assess the performance of the proposed hybrid modeling approach [51]. The spatial locations of these study areas are illustrated in Fig. (**1**). The three case studies were selected based on the closest available gauging stations to nearby cities, towns, and villages, ensuring relevance to urban and peri-urban water management while maintaining high-quality observational data. Station 11264500 is located approximately 80 km from Merced, California, represents a semi-arid region where precipitation forecasting is critical for urban water supply planning, reservoir operation, and drought preparedness [52]. Station 07083000, located in about 10 km from Leadville, Colorado, reflects a high-elevation mountain setting where accurate precipitation prediction supports flood mitigation, stormwater management, and infrastructure resilience under snow-dominated and rapidly changing hydrologic conditions [53]. Station 01013500 located only 2 km from Fort Kent, Maine, represents a cold-region community where precipitation variability influences urban drainage performance, flood risk, and seasonal infrastructure stress [54]. Although the study basins are not strictly urban, selecting gauging stations near populated areas allows the proposed precipitation forecasting framework to be directly transferable to urban and peri-urban applications, supporting climate-resilient water management across diverse settlement types.

Therefore, we will leverage these established case studies to benchmark the results of integrating MODWET with deep learning models [47]. The dataset extracted for this analysis spans the period from January 1980 to December 2014, yielding 420 monthly time steps. It includes 5 climatological variables (Streamflow, solar radiation, maximum/minimum temperature, vapor pressure) as well as 5 large-scale climate indices, each with 12 lagged values (Arctic Oscillation (AO), North Atlantic Oscillation (NAO), ENSO indices (Niño 3, Niño 3.4, Niño 4, Niño 1+2), Pacific Decadal Oscillation (PDO), Pacific-North American Pattern (PNA)) [55]. Additionally, we incorporated 2 Cyclic Seasonal Index (CSI) features to capture the periodic anomalies in the target streamflow data [56].

The selected variables represent key atmospheric and hydrological processes that directly influence precipitation and its impact on urban systems. Precipitation (Prcp.) is the primary driver of urban runoff and stormwater infrastructure performance. Solar radiation (Srad.) and air temperature (T_{max}, T_{min}) control surface energy balance and atmospheric stability, influencing convective rainfall and urban heat island effects. Vapor pressure (VP) reflects atmospheric moisture availability, a critical factor in precipitation formation. Streamflow (Str.Flow) integrates watershed response to precipitation and is essential for understanding urban flood risk and

supporting precipitation-driven urban hydrologic and drainage models. Statistical characteristics of all data sets are presented in Table **1**.

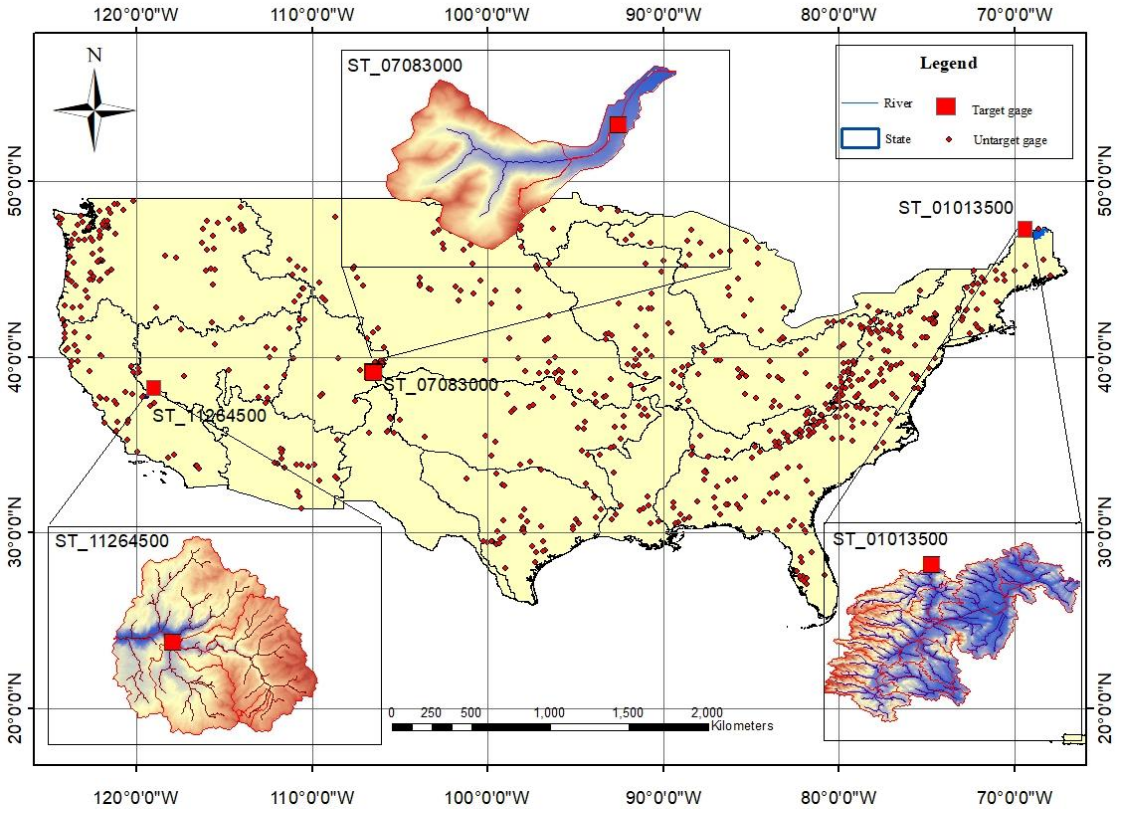

Figure 1: Spatial distribution of CAMELS hydrometeorological stations across the conterminous United States, highlighting the three target study basins: ST_11264500, ST_07083000, and ST_01013500. Red squares indicate the target gauging stations used in this study, while red dots represent other CAMELS stations. Insets show the corresponding watershed boundaries and river networks for each target basin.

Table 1: Summary statistics (maximum, minimum, mean, and standard deviation) of monthly precipitation (Prcp.), solar radiation (Srad.), maximum and minimum air temperature (T_{max}, T_{min}), vapor pressure (VP), and streamflow (Str.Flow) for the three CAMELS hydrometeorological stations used in this study.

Station	Variable	Prcp (mm/day)	Srad (W/m2)	Tmax (C)	Tmin (C)	VP (Pa)	StrFlow (m3/s)
11264500	Max	20.37	731	22.8	11.4	940	3317
	Min	0.00	212	-2.7	-11.5	196	3
	Average	2.65	455	9.3	-1.6	423	373
	SD	3.47	141	6.7	5.6	126	547
7083000	Max	6.71	731	20.7	5.1	799	247
	Min	0.00	235	-7.3	-21.8	116	2
	Average	2.13	467	5.9	-8.3	344	30
	SD	1.23	130	7.6	7.7	166	43
1013500	Max	8.79	569	25.7	13.9	1624	8062
	Min	0.20	118	-12.9	-26.2	87	66
	Average	3.11	302	9.2	-2.5	670	1543
	SD	1.38	112	11.2	10.8	430	1506

3. Methodology

3.1. Gated Recurrent Units

Deep learning models have emerged as powerful tools for precipitation forecasting due to their ability to capture complex, nonlinear, and nonstationary relationships inherent in hydroclimatic time series. Unlike traditional statistical or physically based models, deep learning architectures can learn temporal dependencies directly from data without requiring explicit assumptions about underlying processes. Recurrent neural networks and their variants are particularly well suited for precipitation prediction, as they effectively model long-term dependencies and multi-scale variability. These capabilities make deep learning models especially valuable for forecasting precipitation under changing climatic conditions, where conventional approaches often struggle to maintain predictive accuracy [57].

GRU is a type of recurrent neural network (RNN) architecture designed to effectively model sequential data and improve the traditional RNNs [58]. GRU is particularly adept at capturing long-term dependencies in sequences while mitigating the vanishing gradient problem, which is a common issue in traditional RNNs where gradients diminish over time, hindering learning. GRUs achieve this through a gating mechanism comprising an update gate and a reset gate. The update gate controls the extent to which past information is retained and incorporated into the current context, while the reset gate determines the influence of past information on the current hidden state. This dual gating mechanism enables GRUs to dynamically adjust their memory, selectively updating or discarding information as needed based on the input sequence. Compared to LSTM networks, GRUs have a lower computational expense [59, 60].

In equations 1-4, r_t, u_t, $\hat{h}_t$ and h_t are reset gate, update gate, candidate hidden state and hidden state, respectively. Figure 2 presents the architecture of GRU model.

$$r_t = \sigma(W_{r,x}X_t + W_{r,h}h_{t-1} + b_r) \quad (1)$$

$$u_t = \sigma(W_{u,x}X_t + W_{u,h}h_{t-1} + b_u) \quad (2)$$

$$\hat{h}_t = tanh(W_{g,x}X_t + W_{g,h}(r_t.h_{t-1}) + b_g) \quad (3)$$

$$h_t = u_t.h_{t-1} + (1 - u_t).\hat{h}_t \quad (4)$$

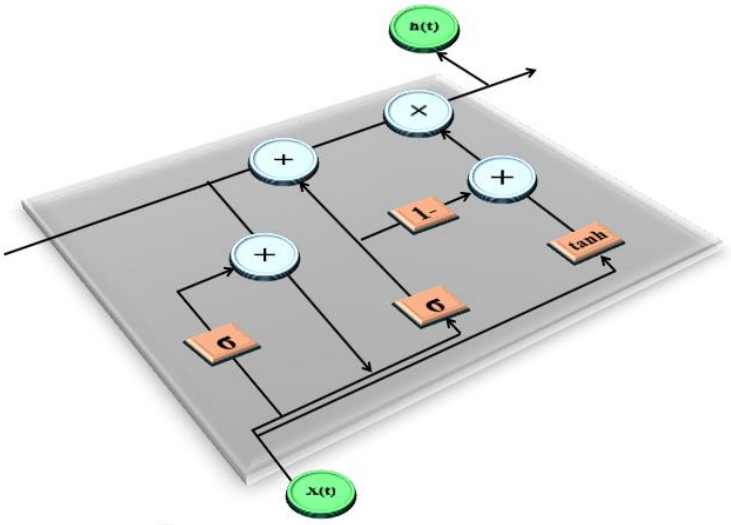

Figure 2: Schematic architecture of a Gated Recurrent Unit (GRU) cell, illustrating the update and reset gates that regulate information flow between the input $x(t)$and the hidden state $h(t)$. The gating mechanisms enable the GRU to capture temporal dependencies by selectively retaining or updating past information.

3.2. MODWET

The objective of signal decomposition is to enhance meaningful features while reducing noise contamination in time-series data. In practice, traditional preprocessing techniques frequently underperform due to inappropriate or heuristic selection of wavelet filters and decomposition levels. MODWET, introduced by, addresses these issues by employing an entropy-based approach to optimize wavelet decomposition levels and filter choices [47].

Entropy quantifies the degree of uncertainty or information content associated with a random process. Within the MODWET framework, entropy serves as an objective criterion for selecting the wavelet filter and decomposition level that retain the most informative signal structure while avoiding unnecessary complexity. Equation 5 illustrates Shannon Entropy [61], where E represents information entropy, X represents a random variable or a time series, N represents the length of time series, and $p(x_i)$ represents the probability of occurrence of x_i.

$$E(x) = -\sum_{i=1}^{n} p(x_i)\, log[p(x_i)] \tag{5}$$

An event with absolute certainty has an entropy value of zero, while a completely random event has an entropy value of one. Within the MODWET framework, this principle is utilized to systematically evaluate multiple wavelet filters and decomposition depths, selecting the configuration that yields the lowest entropy. A minimum entropy value indicates that additional decomposition does not contribute new or informative signal content. The following outlines the MODWT equations (6-8), which incorporate entropy. These equations demonstrate the wavelet coefficient, scaling coefficient, and reconstruction coefficient, respectively Here, (t) denotes the time index, (j) represents the decomposition level, (L) denotes the length of the wavelet filter, and (N) represents the length of the recorded data, and $\tilde{h}_l$ ($\tilde{g}_l$) represents the wavelet (scaling) filter [47].

$$\widetilde{W}_{j,t} = \sum_{l=0}^{L-1} \tilde{h}_l \tilde{V}_{j-1,(t-2^{j-1}l)\ mod\ N} \tag{6}$$

$$\tilde{V}_{j,t} = \sum_{l=0}^{L-1} \tilde{g}_l \tilde{V}_{j-1,(t-2^{j-1}l)\ mod\ N} \tag{7}$$

$$\tilde{V}_{j-1,t} = \sum_{l=0}^{L-1} \tilde{h}_l \widetilde{W}_{j,(t+2^{j-1}l)\ mod\ N} + \sum_{l=0}^{L-1} \tilde{g}_l \tilde{V}_{j,(t+2^{j-1}l)\ mod\ N} \tag{8}$$

Through iterative processes, the filter and decomposition level with the lowest entropy value for the wavelet and scaling coefficients are determined. The appropriate decomposition level and filter are selected based on the following conditions (Eq. 10-12):

Step 1): $$L_J << N \text{ , (UL)} \tag{9}$$

$$L(J) = (2^J - 1)(L - 1) + 1 \tag{10}$$

Step 2): $$Entropy_{a,d}(j) < Entropy_a(j-1), \text{(LL)} \tag{11}$$

Step 3): $$Min(Entropy\ max <_{Jmax} \tag{12}$$

The flowchart depicting the decomposition process using MODWET and its application in precipitation forecasting is presented in Fig. (**3**). MODWET is specifically tailored for streamflow forecasting and involves decomposing input data using wavelet transformers. Unlike traditional wavelet transforms, MODWET employs a maximal overlap scheme, allowing for a more thorough analysis of the input signal. By calculating discrete wavelet entropy on the decomposed components, MODWET captures the complexity and information content of streamflow data, enhancing the accuracy and reliability of forecasts by integrating with various machine learning models. While the effectiveness of MODWET in streamflow forecasting has been demonstrated, its potential in combination with deep learning models remains an area for future research, which is the primary objective of this paper [47].

3.3. Experiment Design

To forecast precipitation, we utilized data spanning from January 1980 to December 2014. This dataset was split into two portions: 70% for training and 30% for testing. A t-test was conducted to ensure that partitioning was

appropriate by comparing the training and testing datasets for similarity [62]. The training data was then processed using the MODWET, which decomposes the time series data into frequency domain components, as detailed in Section 3.2.

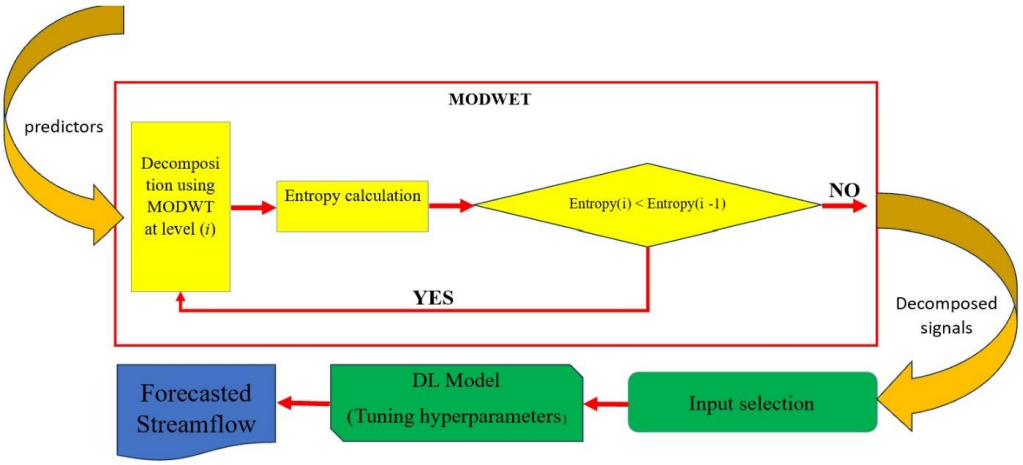

Figure 3: Flowchart of the proposed PCI–MODWET–GRU forecasting framework. Predictor variables are first decomposed using the Maximal Overlap Discrete Wavelet Entropy Transform (MODWET), where entropy is evaluated iteratively across decomposition levels to identify the optimal wavelet representation. The resulting decomposed signals are then subjected to input selection, followed by deep learning model training and hyperparameter tuning, leading to the final precipitation (or streamflow) forecast.

PCI feature selection procedure was applied to determine the most informative predictors, including their 12-month lagged values and wavelet-decomposed components. This method was applied in parallel to assess their effectiveness separately [63, 64]. Table **2** lists the features and their lags selected by this method, highlighting that solar radiation, precipitation, and vapor pressure—decomposed using MODWET—were chosen by the feature selection models. This table indicates that PCI selected fewer datasets, reducing computational load and speeding up the forecasting process. It is important to note that long lags can also be useful for forecasting, as shown in Table **2**.

Based on the predictors selected by the PCI method, a GRU deep learning model was developed to forecast monthly precipitation. Model hyperparameters were optimized during the training stage, with the tuning results summarized in Section 4.1. The predictive performance of the GRU model, both with and without MODWET preprocessing, was then evaluated using RMSE, PBIAS, NSE, MAE, r^2 and standard deviation. Table **3** provides a summary of all the elements applied in this study.

4. Results and Discussion

4.1. Hyper Parameters Tuning

in our deep learning models, we optimized several hyperparameters to enhance performance. The parameters under consideration are provided in Table **3**. We employed a trial-and-error method to optimize each hyperparameter sequentially. This approach involved adjusting one parameter at a time while keeping the others constant to observe its impact on model performance. The results indicate that each model and case study has an individual set of optimal parameters. Moreover, one hidden layer proved to be the best configuration across all models and case studies. Notably, the Adam optimizer demonstrated superior performance in 4 out of 6 cases. It outperformed particularly in stations with substantial streamflow values. However, for station 07083000, which has lower streamflow value, SGD emerged as the definitive best choice. However, the suitable activation function for station 07083000 is different from the other stations like optimizer. It seems that MSE suits this station more than others.

Table 2: Results of PCI-based input selection showing the most influential predictors and their associated lag times for Stations 01013500, 07083000, and 11264500. Selected inputs include raw hydroclimatic variables, climate indices, and entropy-guided wavelet-decomposed components incorporated into the deep learning model.

Station 01013500		Station 07083000		Station 11264500	
PCI	**Lag (Month)**	**PCI**	**Lag (Month)**	**PCI**	**Lag (Month)**
StrFlow	1-2-8-9	vp	1-2-3-4-5-6-7-8-10-11	prcp	1-2-3-4-5-6-7-8-9-10-11
tmax	3-6-7	StrFlow	1-2-3-4-5-6-7-8-12	StrFlow	1-2-3-4-5-6-7-8
tmin	4-6	tmin	9-10	srad	9-12
vp	6-9-10	tmax	10	tmax	13
PNA	1-6-9-13	PNA	1-2-10-13	tmin	13
AO	4-7-8-9	NAO	3-4	PNA	1-10-11
NAO	7-9-12	AO	4-6	AO	7
PDO	13	PDO	13	NAO	11-13
srad_fk4_J3_W3	1	prcp_db5_J1_V1	1	PDO	13
srad_fk4_J3_V3	1	srad_fk4_J3_W1	1	prcp_db5_J1_V1	1
CSI-S	1	Vp_db1_J1_W1	1	srad_fk4_J3_W1	1
CSI-C	1	Vp_db1_J1_V1	1	Vp_db1_J1_W1	1
		CSI-S	1	Vp_db1_J1_V1	1
		CSI-C	1		

Table 3: Optimal hyperparameter configurations obtained through model tuning for the PCI-GRU and MODWET-PCI-GRU models across the three study stations. Reported parameters include the optimizer, learning rate, batch size, loss function, activation function, network depth, number of hidden nodes, and training epochs.

Station	1013500		7083000		11264500	
Model	**PCI-GRU**	**MODWET-PCI-GRU**	**PCI-GRU**	**MODWET-PCI-GRU**	**PCI-GRU**	**MODWET-PCI-GRU**
Optimizer	Adam	Adam	SGD	SGD	Adam	Adam
Learning rate	0.01	0.001	0.1	0.001	0.1	0.1
Batch size	16	16	32	16	16	16
Loss function	MSE	huber_loss	MSE	MSE	huber_loss	huber_loss
Activation function	softmax	softmax	softsign	Relu	softmax	softmax
Number of hidden layers	1	1	1	1	1	1
Number of nodes in hidden layer	10	32	32	64	64	64
Number of epochs	250	350	250	200	350	350

4.2. Model Performance Evaluation

The findings revealed that MODWET selects different optimal wavelet filters and decomposition levels for various datasets as provided in Table **2**. For instance, solar radiation was decomposed into three levels using the fk4 wavelet filter, whereas vapor pressure and precipitation were each decomposed into one level with the db1 wavelet filter across all three stations. This diversity indicates that a single wavelet filter and decomposition level

cannot be universally applied to all datasets and stations in this study. Instead, MODWET effectively identifies the most suitable filter and decomposition level for each specific case. The accuracy results are presented in Table **4**.

Table 4: Statistical performance of the PCI-GRU and PCI-MODWET-GRU models for monthly precipitation forecasting across the three study stations during the testing and training periods. Model performance is evaluated using RMSE, Nash–Sutcliffe efficiency (NSE), coefficient of determination (r^2), mean absolute error (MAE), and percent bias (PBIAS).

Station	Model	Test					Train				
		RMSE	NSE	r^2	MAE	PBIAS	RMSE	NSE	r^2	MAE	PBIAS
1013500	PCI-GRU	0.13	0.23	0.48	0.11	2.03	0.15	0.15	0.44	0.11	-9.31
	PCI-MODWET-GRU	0.12	0.34	0.59	0.1	1.31	0.15	0.15	0.48	0.11	-6.89
7083000	PCI-GRU	0.16	0.28	0.54	0.13	3.79	0.17	-0.05	0.28	0.14	-15.8
	PCI-MODWET-GRU	0.15	0.38	0.63	0.12	5.31	0.17	0.06	0.33	0.13	-1.28
11264500	PCI-GRU	0.12	0.5	0.71	0.08	-3.16	0.16	-0.13	0.47	0.11	48.6
	PCI-MODWET-GRU	0.11	0.58	0.78	0.08	-13.07	0.14	0.09	0.49	0.1	16.57

In Station 01013500, the PCI-MODWET-GRU model consistently outperforms the PCI-GRU model across all metrics, indicating the effectiveness of the MODWET preprocessing in enhancing the model's predictive capability (Fig. **4**). The PBIAS values show a negative bias for both models, with PCI-MODWET-GRU showing an underestimated result, which could be due to down trending precipitation in this station. The PCI-GRU Compared to the PCI-MODWET-GRU achieved an NSE of 0.23, the PCI-MODWET-GRU model in this analysis shows a higher NSE (0.34). This indicates that the MODWET-GP-GRU model might perform better at this station. The similar RMSE and MAE values for the train and test sets suggest no significant overfitting in the PCI-MODWET-GRU model. These results are particularly relevant for Fort Kent, a community historically affected by riverine flooding from the Fish and St. John Rivers, where flood events have inundated roads and properties in the past and motivated the construction of local flood protection projects. Reliable monthly precipitation forecasts around this town can support better timing of reservoir releases and flood control operations, inform stormwater and emergency response planning, and guide the design of resilient infrastructure and land-use strategies that reduce flood risk for residents and protect the local economy [65].

In the Station 07083000, the PCI-MODWET-GRU model again shows superior performance compared to the PCI-GRU model, especially in terms of NSE and r^2. The PBIAS values indicate a stronger negative bias in predictions for this station, which is somewhat mitigated by the PCI-MODWET-GRU model. The PCI-GRU Compared to the PCI-MODWET-GRU achieved an NSE of 0.28, the PCI-MODWET-GRU model in this analysis shows a higher NSE (0.38). This indicates that the MODWET-GP-GRU model might have better performance at this station. These results are particularly relevant for Leadville, Colorado, a high-elevation mountain town where precipitation variability, snowmelt-driven runoff, and seasonal transitions strongly influence urban hydrology. Improved monthly precipitation forecasts can support the design of resilient drainage systems, road infrastructure, and snowmelt management strategies by informing capacity planning and maintenance scheduling. Such information is valuable for climate-responsive urban design and long-term water resource planning in cold-region communities where infrastructure must accommodate both rainfall and snowmelt processes.

In the Station 11264500, the PCI-MODWET-GRU model shows substantial improvement over the PCI-GRU model in terms of NSE, r^2, PBIAS and MAE, highlighting the effectiveness of MODWET preprocessing. The PCI-GRU Compared to the PCI-MODWET-GRU achieved an NSE of 0.50, the PCI-MODWET-GRU model in this analysis shows a higher NSE (0.58). This indicates that the MODWET-GP-GRU model have a better performance at this station. These performance improvements are particularly relevant for the Merced, California region, where precipitation variability influences urban drainage performance, flood risk, and water supply reliability in an agricultural–urban setting. More accurate monthly precipitation forecasts can support the design and operation of stormwater infrastructure, groundwater recharge facilities, and flood mitigation measures, especially during wet-season

events. The enhanced predictive skill demonstrated by the PCI–MODWET–GRU model therefore provides valuable information for climate-responsive urban and water infrastructure planning in the Merced area.

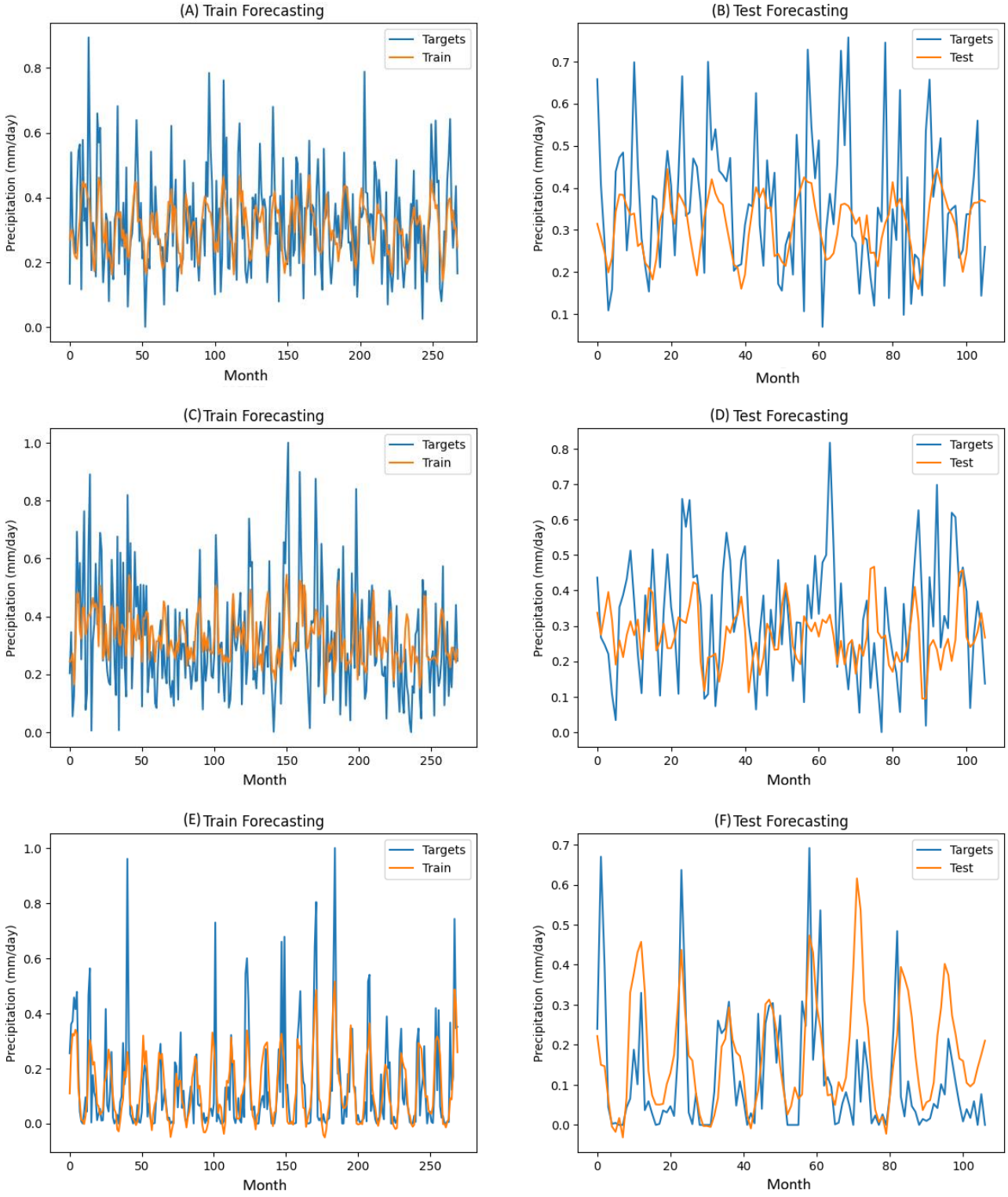

Figure 4: The results of PCI-GRU modeling for train and test. (A and B) station 01013500, (C and D) station 07083000 and (E and F) station 11264500.

Overall, the PCI-MODWET-GRU model consistently outperforms the PCI-GRU model across all stations in terms of RMSE, NSE, r^2, and MAE, underscoring the benefits of using MODWET for preprocessing. Bias varies across stations, with the highest positive bias observed at Station 11264500 and the highest negative bias at Station

07083000, it indicates that models like PCI-MODWET-GRU might outperform PCIGRU, especially in terms of NSE values. Overfitting or data anomalies are a concern at Station 07083000, as indicated by the disparity in RMSE values between the train and test sets.

Fig. (**4**) (PCI-GRU) and 5 (MODWET-PCI-GRU) present the plot of precipitation forecasting for all the three stations. Fig. (**4**) illustrates the training and testing results of the PCI-GRU model for monthly precipitation forecasting across the three study stations. Overall, the PCI-GRU model can capture the general temporal patterns and seasonal variability of precipitation at all stations, with a reasonable agreement between observed and simulated values during both the training and testing periods. However, noticeable discrepancies remain, particularly during peak precipitation events, where the model tends to smooth extremes and underestimate higher magnitudes. These deviations are more pronounced during the testing phase, indicating the limitations of the standalone GRU model when trained on raw or partially processed inputs. The figure highlights residual noise and reduced accuracy in reproducing sharp fluctuations, underscoring the need for enhanced preprocessing strategies to better represent multi-scale precipitation dynamics, which motivates the integration of MODWET in the subsequent modeling framework.

Fig. (**5**) presents the training and testing results of the MODWET-PCI-GRU model for monthly precipitation forecasting at the three study stations. Compared to the standalone PCI-GRU model, the MODWET-enhanced framework shows a visibly improved agreement between observed and simulated precipitation, particularly in capturing seasonal patterns and reducing high-frequency noise. The incorporation of MODWET leads to smoother predictions that more closely follow the observed temporal dynamics, with improved representation of both rising and falling precipitation trends. While some underestimation of extreme peaks persists, the MODWET-PCI-GRU model demonstrates a clearer ability to preserve dominant signal structures and reduce spurious fluctuations during both training and testing periods. These visual improvements are consistent with the quantitative performance gains reported in Table **4**, confirming the effectiveness of entropy-guided wavelet preprocessing in enhancing deep learning-based precipitation forecasting.

4.3. Implications for Urban Architecture and Climate-Responsive Design

From an urban architecture and design standpoint, precipitation forecasting plays a fundamental role in shaping climate-responsive and resilient built environments [66, 67]. Rainfall patterns directly influence the design of building envelopes and site drainage layouts, as well as the integration of green infrastructure such as green roofs, permeable pavements, rain gardens, and urban open spaces. At the neighborhood and city scale, precipitation projections inform stormwater conveyance capacity, flood-safe building placement, and the spatial organization of critical infrastructure. Reliable monthly precipitation forecasts are particularly important during early design and planning stages, where long-term climatic tendencies guide material selection, structural detailing, and water-sensitive urban design strategies rather than short-term operational decisions.

Accurate precipitation forecasting also supports adaptive urban design under climate change by enabling architects and planners to anticipate shifts in rainfall variability and intensity [68]. As cities face increasing exposure to waterlogging, pluvial flooding, and infrastructure overstress, data-driven precipitation forecasts provide essential inputs for performance-based design approaches and resilience assessments. In this context, models capable of capturing nonstationary precipitation behavior and seasonal variability are especially valuable, as they help translate climatic uncertainty into actionable design constraints and opportunities at both building and district scales [69, 70].

The proposed PCI–MODWET–GRU modeling framework demonstrates performance characteristics that align well with these urban architectural needs. By effectively capturing dominant precipitation trends and seasonal patterns while reducing noise, the model provides stable and interpretable forecasts suitable for planning-oriented applications. Although some underestimation of extreme precipitation events remains, the improved signal representation achieved through entropy-guided preprocessing enhances reliability at the monthly scale most relevant to urban design decisions. This balance between accuracy and stability makes the proposed framework particularly suitable for supporting climate-resilient urban architecture and water-sensitive design strategies, where understanding long-term precipitation behavior is often more critical than resolving short-

duration extremes. Section 4.3.1 presents an illustrative example demonstrating how the results of this study can be applied in practice.

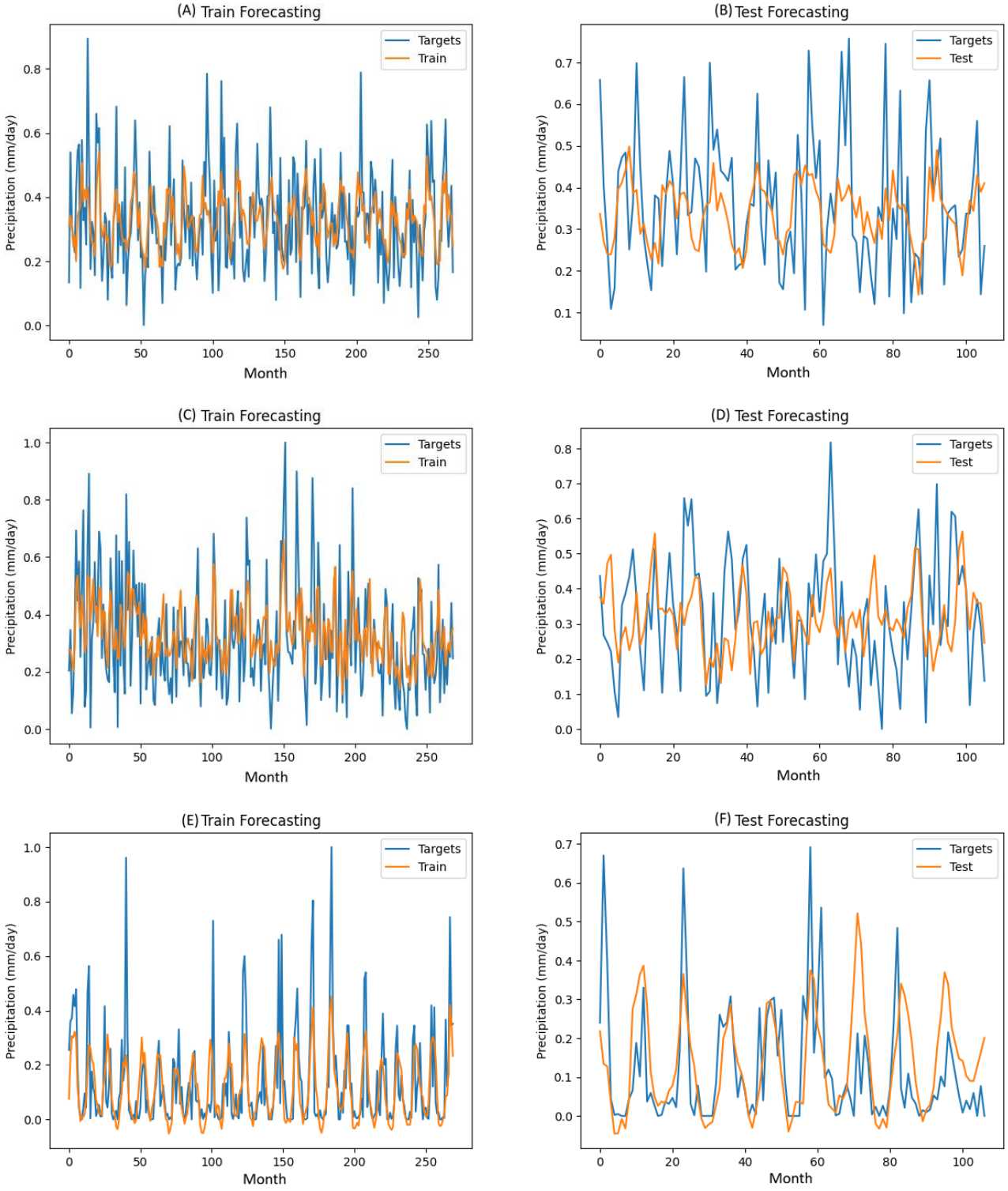

Figure 5: The results of MODWET-PCI-GRU modeling for train and test. (A and B) station 01013500, (C and D) station 07083000 and (E and F) station 11264500.

4.3.1. Illustrative Application: Planning the Sizing of an Underground Stormwater Conduit

To directly demonstrate how the proposed monthly precipitation forecasting framework can support urban infrastructure planning, we provide a planning-stage example showing how model outputs can be translated into

stormwater conveyance capacity and an indicative underground pipe diameter. This example is intentionally simplified and is not intended to replace detailed local design procedures (e.g., site-specific IDF curves, time of concentration analysis, SWMM modeling, inlet control, surcharge checks). Rather, it provides a transparent link between monthly forecasts and a tangible urban design variable (drainage conduit sizing). Station precipitation statistics (mean precipitation (mm/day)) are taken from Table **1**: Station 11264500 = 2.65, Station 07083000 = 2.13, Station 01013500 = 3.11 and model bias (PBIAS, %) is taken from Table **4** (test period). Using the model PBIAS, the predicted precipitation is calculated (Eq. 13 and 14).

$$\mathrm{PBIAS} = 100 \times \frac{\sum(P_{\mathrm{pred}} - P_{\mathrm{obs}})}{\sum P_{\mathrm{obs}}} \tag{13}$$

$$\overline{P}_{\mathrm{pred}} = \overline{P}_{\mathrm{obs}} \left(1 + \frac{\mathrm{PBIAS}}{100}\right) \tag{14}$$

Because drainage capacity depends on intensity (mm/hr), we convert the predicted mean daily precipitation to an average hourly intensity and apply a peaking factor k (Eq. 15) as the drainage channels design are based on the precipitation peak not the average precipitation [71]:

$$i_{\mathrm{design}} = k \left(\frac{\overline{P}_{\mathrm{pred}}}{24}\right) \ [\mathrm{mm\ hr^{-1}}] \tag{15}$$

Finally, we convert design intensity to peak discharge (Rational method) (Eq. 16) [72]:

$$Q_{\mathrm{peak}} = 0.00278\, C\, i_{\mathrm{design}}\, A \ [\mathrm{m^3\ s^{-1}}] \tag{16}$$

Where *A* is drainage area in hectare and *C* is the runoff coefficient. In the final step we determine the size of an underground conduit using Manning equation (as a simple model) for full circular pipe (Eq. 17) [72]:

$$Q_{\mathrm{peak}} = \frac{1}{n}\, A_p\, R_h^{2/3}\, S^{1/2} \tag{17}$$

Where n is Manning roughness coefficient, A_p is the wetted cross-sectional area $[\mathrm{m}^2]$, R_h is hydraulic radius $[\mathrm{m}]$ and S is channel bed slope. By assuming $k = 20$, $A = 20\mathrm{ha}$, $C = 0.70$, $n = 0.013$ and $S = 0.005$. The results of drainage diameter design for the three cases are provided in Table **5**.

Table 5: Planning-stage underground stormwater conduit sizing derived from predicted precipitation produced by the PCI-GRU and PCI–MODWET–GRU models for the three study stations. Predicted mean daily precipitation is converted to a design rainfall intensity using a consistent peaking factor, and peak discharge is estimated using the Rational method. Indicative conduit diameters are then obtained by solving Manning's equation for full-flow conditions under representative urban drainage assumptions. The results illustrate how differences in precipitation forecasts propagate into urban drainage capacity requirements at the planning stage.

Town	Station	Model	$\overline{P}_{pred}(mm/day)$	$i_{design}(mm/hr)$	$Q_{peak}(m^3/s)$	$Pipe\ D\ (m)$
Fort Kent	1013500	PCI-GRU	3.17	2.64	0.10	0.35
		PCI–MODWET–GRU	3.15	2.63	0.10	0.35
Leadville	7083000	PCI-GRU	2.21	1.84	0.07	0.31
		PCI–MODWET–GRU	2.24	1.87	0.07	0.31
Merced	11264500	PCI-GRU	2.57	2.14	0.08	0.32
		PCI–MODWET–GRU	2.30	1.92	0.07	0.31

This example provides a transparent pathway from monthly precipitation predictions to stormwater conveyance design variables. Even modest differences in predicted precipitation between PCI-GRU and PCI–MODWET–GRU lead to measurable differences in computed peak discharge and indicative pipe diameter. For

instance, at Station 11264500, the lower predicted precipitation level implied by PCI–MODWET–GRU yields a smaller planning-stage diameter (0.31 m) than PCI-GRU (0.32 m), illustrating how forecast outputs can propagate into infrastructure capacity decisions.

The largest required conduit diameter occurs at Station 01013500 (Fort Kent, Maine), which consistently exhibits the highest mean precipitation among the three case studies. This station is in a cold-region hydrologic setting where frequent precipitation, combined with seasonal snow accumulation and snowmelt-driven runoff, contributes to elevated effective runoff volumes during wet periods. As a result, even under identical urban catchment and design assumptions, the higher predicted precipitation levels at Fort Kent translate into larger design rainfall intensities and peak discharges, necessitating increased conveyance capacity. This highlights the importance of accounting for regional climatic characteristics when translating precipitation forecasts into urban drainage design requirements.

5. Conclusion

This study investigated the effectiveness of integrating MODWET as a preprocessing framework with a GRU deep learning model for monthly precipitation forecasting. In addition, the PCI was employed as an input selection method to reduce predictor redundancy and prevent the inclusion of non-informative variables, thereby improving model parsimony and computational efficiency. The proposed hybrid framework was evaluated across three hydrometeorological stations close to urbane area from the CAMELS dataset to assess its robustness and generalizability under different hydroclimatic settings relevant to planning- and design-oriented water management applications.

The results consistently demonstrate that incorporating MODWET into the GRU architecture leads to improved predictive performance compared to the standalone GRU model at all three stations. This improvement is evident across multiple evaluation metrics, including RMSE, NSE, MAE, and correlation coefficient, confirming that entropy-guided wavelet decomposition enhances the representation of nonstationary and multi-scale precipitation signals prior to deep learning. Among the examined stations, 01013500 and 11264500 exhibited the highest predictive skill, with correlation coefficients approaching 0.49, indicating a strong agreement between observed and simulated precipitation. These findings suggest that the proposed PCI–MODWET–GRU framework is particularly effective in regions where precipitation exhibits pronounced temporal structure and climatic forcing. Despite the overall performance gains, the results also reveal a systematic underestimation at two of the three stations, particularly during higher-magnitude precipitation events. This behavior suggests that, while MODWET improves signal decomposition and noise reduction, challenges remain in fully capturing extreme precipitation dynamics using data-driven deep learning models alone. Such underestimation may be attributed to the limited representation of extremes in the training data, the smoothing effect of wavelet decomposition, or the inherent difficulty of learning rare events in monthly-scale precipitation records.

Overall, this study presents the first comprehensive evaluation of MODWET applied to precipitation forecasting within a deep learning framework. The results demonstrate that entropy-based preprocessing combined with targeted input selection can substantially enhance the performance and interpretability of deep learning models for hydroclimatic time series. From an urban design and architectural perspective, improved reliability in monthly precipitation forecasting supports climate-responsive planning, water-sensitive urban design, and the integration of green and blue infrastructure into the built environment. Future research should extend this framework to higher temporal resolutions, incorporate physics-informed constraints, and adopt extreme-event-aware loss functions to further reduce bias and strengthen robustness under evolving climate conditions. The proposed hybrid approach therefore offers a promising pathway toward more dependable precipitation forecasting tools that can inform urban infrastructure design, resilient architecture, and long-term water management strategies.

Conflict of Interest

The authors declare that there are no conflicts of interest regarding the publication of this paper.

Funding

This work did not receive any specific funding from public, commercial, or not-for-profit agencies.

References

[1] Agonafir C, Lakhankar T, Khanbilvardi R, Krakauer N, Radell D, Devineni N. A review of recent advances in urban flood research. Water Secur. 2023; 19: 100141. https://doi.org/10.1016/j.wasec.2023.100141

[2] Fletcher TD, Shuster W, Hunt WF, Ashley R, Butler D, Arthur S, *et al*. SUDS, LID, BMPs, WSUD and more – The evolution and application of terminology surrounding urban drainage. Urban Water J. 2015; 12(7): 525-42. https://doi.org/10.1080/1573062X.2014.916314

[3] Ma XY, Wang XC. Ecotoxicity comparison of organic contaminants and heavy metals using Vibrio-qinghaiensis sp.-Q67. Water Sci Technol. 2013; 67(10): 2221-7. https://doi.org/10.2166/wst.2013.113

[4] Jha AK, Bloch R, Lamond J. Cities and flooding: a guide to integrated urban flood risk management for the 21st century. Washington, DC: World Bank; 2012. https://doi.org/10.1596/978-0-8213-8866-2

[5] Milly PCD, Betancourt J, Falkenmark M, Hirsch RM, Kundzewicz ZW, Lettenmaier DP, *et al*. Stationarity is dead: whither water management? Science. 2008; 319(5863): 573-4. https://doi.org/10.1126/science.1151915

[6] Meerow S, Newell JP, Stults M. Defining urban resilience: A review. Landsc Urban Plan. 2016; 147: 38-49. https://doi.org/10.1016/j.landurbplan.2015.11.011

[7] Emmanuel R, Loconsole A. Green infrastructure as an adaptation approach to tackling urban overheating in the Glasgow Clyde Valley Region, UK. Landsc Urban Plan. 2015; 138: 71-86. https://doi.org/10.1016/j.landurbplan.2015.02.012

[8] Kinnane O, Sinnott D, Turner WJN. Evaluation of passive ventilation provision in domestic housing retrofit. Build Environ. 2016; 106: 205-18. https://doi.org/10.1016/j.buildenv.2016.06.032

[9] Wong THF, Brown RR. The water sensitive city: principles for practice. Water Sci Technol. 2009; 60(3): 673-82. https://doi.org/10.2166/wst.2009.436

[10] Campbell T. Learning cities: Knowledge, capacity and competitiveness. Habitat Int. 2009; 33(2): 195-201. https://doi.org/10.1016/j.habitatint.2008.10.012

[11] Ortiz J, Fonseca i Casas A, Salom J, Garrido Soriano N, Fonseca i Casas P. Cost-effective analysis for selecting energy efficiency measures for refurbishment of residential buildings in Catalonia. Energy Build. 2016; 128: 442-57. https://doi.org/10.1016/j.enbuild.2016.06.059

[12] Czemiel Berndtsson J. Green roof performance towards management of runoff water quantity and quality: A review. Ecol Eng. 2010; 36(4): 351-60. https://doi.org/10.1016/j.ecoleng.2009.12.014

[13] Zhou Q. A review of sustainable urban drainage systems considering the climate change and urbanization impacts. Water. 2014; 6(4): 976-92. https://doi.org/10.3390/w6040976

[14] Meerow S, Newell JP. Spatial planning for multifunctional green infrastructure: Growing resilience in Detroit. Landsc Urban Plan. 2017; 159: 62-75. https://doi.org/10.1016/j.landurbplan.2016.10.005

[15] Santana MV, Zhang Q, Nachabe MH, Xie X, Mihelcic JR. Could smart growth lower the operational energy of water supply? A scenario analysis in Tampa, Florida, USA. Landsc Urban Plan. 2017; 164: 99-108. https://doi.org/10.1016/j.landurbplan.2017.04.010

[16] Geneletti D, Zardo L. Ecosystem-based adaptation in cities: An analysis of European urban climate adaptation plans. Land Use Policy. 2016; 50: 38-47. https://doi.org/10.1016/j.landusepol.2015.09.003

[17] Ahiablame LM, Engel BA, Chaubey I. Effectiveness of Low Impact Development Practices: Literature Review and Suggestions for Future Research. Water Air Soil Pollut. 2012; 223(7): 4253-73. https://doi.org/10.1007/s11270-012-1189-2

[18] Demuzere M, Orru K, Heidrich O, Olazabal E, Geneletti D, Orru H, *et al*. Mitigating and adapting to climate change: Multi-functional and multi-scale assessment of green urban infrastructure. J Environ Manage. 2014; 146: 107-15. https://doi.org/10.1016/j.jenvman.2014.07.025

[19] Hathaway JM, Bean EZ, Bernagros JT, Christian DP, Davani H, Ebrahimian A, *et al*. A synthesis of climate change impacts on stormwater management systems: designing for resiliency and future challenges. J Sustain Water Built Environ. 2024; 10(2): 04023014. https://doi.org/10.1061/JSWBAY.SWENG-533

[20] Zellner ML, Massey D. Modeling benefits and tradeoffs of green infrastructure: Evaluating and extending parsimonious models for neighborhood stormwater planning. Heliyon. 2024; 10(5): e27007. https://doi.org/10.1016/j.heliyon.2024.e27007

[21] Nodine TG, Conley G, Riihimaki CA, Holland C, Beck NG. Modeling the impact of future rainfall changes on the effectiveness of urban stormwater control measures. Sci Rep. 2024; 14(1): 4082. https://doi.org/10.1038/s41598-024-53611-1

[22] Meema T, Tachikawa Y, Ichikawa Y, Yorozu K. Real-time optimization of a large-scale reservoir operation in Thailand using adaptive inflow prediction with medium-range ensemble precipitation forecasts. J Hydrol Reg Stud. 2021; 38: 100939. https://doi.org/10.1016/j.ejrh.2021.100939

[23] Specifications and Accuracy of Rainfall Forecast Required for Pre-Release at Multi-Purpose Reservoirs in Japan. (cited 2026 Jan 9). https://doi.org/10.3390/w15071277

[24] Ferdowsi A, Piadeh F, Behzadian K, Mousavi SF, Ehteram M. Urban water infrastructure: A critical review on climate change impacts and adaptation strategies. Urban Clim. 2024; 58: 102132. https://doi.org/10.1016/j.uclim.2024.102132

[25] Dharmarathne G, Waduge AO, Bogahawaththa M, Rathnayake U, Meddage DPP. Adapting cities to the surge: A comprehensive review of climate-induced urban flooding. Results Eng. 2024; 22: 102123. https://doi.org/10.1016/j.rineng.2024.102123

[26] Akinsanola AA, Singhai P, Taguela TN, Folorunsho AH, Adeyeri OE, Morakinyo TE, *et al*. A review of urban resilience to weather and climate extremes. City Built Environ. 2025; 3(1): 24. https://doi.org/10.1007/s44213-025-00063-6

[27] Cuo L, Pagano TC, Wang QJ. A Review of Quantitative Precipitation Forecasts and Their Use in Short- to Medium-Range Streamflow Forecasting. J Hydrometeorol. 2011; 12(5): 713-28. https://doi.org/10.1175/2011JHM1347.1

[28] Briggs MA, Gazoorian CL, Doctor DH, Burns DA. A multiscale approach for monitoring groundwater discharge to headwater streams by the U.S. Geological Survey Next Generation Water Observing System Program—An example from the Neversink Reservoir watershed, New York. Fact Sheet. U.S. Geological Survey; 2022 (cited 2024 Dec 5). Report No.: 2022-3077. https://doi.org/10.3133/fs20223077

[29] Cheung KKW. Bridging the Scaling Gap: A Review of Nonlinear Paradigms for the Estimation and Understanding of Extreme Rainfall from Heavy Storms. Fractal Fract. 2025; 9(12): 827. https://doi.org/10.3390/fractalfract9120827

[30] Koltermann da Silva J, Burrichter B, Niemann A, Quirmbach M. A systematic modular approach for the coupling of deep-learning-based models to forecast urban flooding maps in early warning systems. Hydrology. 2024; 11(12): 215. https://doi.org/10.3390/hydrology11120215

[31] Sham FAF, El-Shafie A, Jaafar WZBW, Adarsh S, Sherif M, Ahmed AN. Improving rainfall forecasting using deep learning data fusing model approach for observed and climate change data. Sci Rep. 2025; 15(1): 27872. https://doi.org/10.1038/s41598-025-13567-2

[32] Zhao X, Wang H, Bai M, Xu Y, Dong S, Rao H, *et al*. A comprehensive review of methods for hydrological forecasting based on deep learning. Water. 2024; 16(10): 1407. https://doi.org/10.3390/w16101407

[33] Chuasuk P, Bhatrasataponkul T, Akkarapongtrakul A. Comparative analysis and enhancing rainfall prediction models for monthly rainfall prediction in the Eastern Thailand. MethodsX. 2025; 14: 103094. https://doi.org/10.1016/j.mex.2024.103094

[34] Sit M, Demiray BZ, Xiang Z, Ewing GJ, Sermet Y, Demir I. A comprehensive review of deep learning applications in hydrology and water resources. Water Sci Technol. 2020; 82(12): 2635-70. https://doi.org/10.2166/wst.2020.369

[35] Behbahani MRM, Rey DM, Briggs MA, Bagtzoglou AC. A spatiotemporal deep learning approach for predicting daily air-water temperature signal coupling and identification of key watershed physical parameters in a montane watershed. J Hydrol. 2025; 663: 134139. https://doi.org/10.1016/j.jhydrol.2025.134139

[36] Gao S, Huang Y, Zhang S, Han J, Wang G, Zhang M, *et al*. Short-term runoff prediction with GRU and LSTM networks without requiring time step optimization during sample generation. J Hydrol. 2020; 589: 125188. https://doi.org/10.1016/j.jhydrol.2020.125188

[37] Łępicki M, Latkowski T, Antoniuk I, Bukowski M, Świderski B, Baranik G, *et al*. Comparative Evaluation of Sequential Neural Network (GRU, LSTM, Transformer) Within Siamese Networks for Enhanced Job–Candidate Matching in Applied Recruitment Systems. Appl Sci. 2025; 15(11): 5988. https://doi.org/10.3390/app15115988

[38] Shi T, Shide K. A comparative analysis of LSTM, GRU, and Transformer models for construction cost prediction with multidimensional feature integration. J Asian Archit Build Eng. 2026; 25(1): 634-49. https://doi.org/10.1080/13467581.2025.2455034

[39] Guo T, Zhang T, Lim E, López-Benítez M, Ma F, Yu L. A Review of Wavelet Analysis and Its Applications: Challenges and Opportunities. IEEE Access. 2022; 10: 58869-903. https://doi.org/10.1109/ACCESS.2022.3179517

[40] Xie J, Chen W, Dai H. Distributed cooperative learning algorithms using wavelet neural network. Neural Comput Appl. 2019; 31(4): 1007-21. https://doi.org/10.1007/s00521-017-3134-1

[41] Abda Z, Zerouali B, Chettih M, Guimarães Santos CA, de Farias CAS, Elbeltagi A. Assessing machine learning models for streamflow estimation: a case study in Oued Sebaou watershed (Northern Algeria). Hydrol Sci J. 2022; 67(9): 1328-41. https://doi.org/10.1080/02626667.2022.2083511

[42] Quilty J, Adamowski J. Addressing the incorrect usage of wavelet-based hydrological and water resources forecasting models for real-world applications with best practices and a new forecasting framework. J Hydrol. 2018; 563: 336-53. https://doi.org/10.1016/j.jhydrol.2018.05.003

[43] Xia YX, Xu RK, Ni YQ, Jin ZQ. Strain signal denoising in bridge SHM: A comparative analysis of MODWT and other techniques. J Infrastruct Intell Resil. 2025; 4(3): 100155. https://doi.org/10.1016/j.iintel.2025.100155

[44] Varghese PR, Subathra MSP, Peter G, Stonier AA, Kuppusamy R, Teekaraman Y. A novel MODWT–local pattern transformation feature fusion approach for high-impedance fault detection in medium voltage power distribution networks. Neural Comput Appl. 2025; 37(22): 17457-71. https://doi.org/10.1007/s00521-024-10863-2

[45] Tahi M, Miloudi A. Rotating machinery faults classification by MODWT and the SVM distribution generated by the genetic wrapper. Aust J Electr Electron Eng. 2025; 1-14. https://doi.org/10.1080/1448837X.2025.2528473

[46] Behbahani MRM, Mazarei M, Bagtzoglou AC. Improving deep learning-based streamflow forecasting under trend varying conditions through evaluation of new wavelet preprocessing technique. Stoch Environ Res Risk Assess. 2024; 38(10): 3963-84. https://doi.org/10.1007/s00477-024-02788-y

[47] Mazarei Behbahani MR, Mazarei A. A new criteria for determining the best decomposition level and filter for wavelet-based data-driven forecasting frameworks- validating using three case studies on the CAMELS dataset. Stoch Environ Res Risk Assess. 2023; 37(12): 4827-42. https://doi.org/10.1007/s00477-023-02531-z

[48] Coifman RR, Wickerhauser MV. Entropy-based algorithms for best basis selection. IEEE Trans Inf Theory. 1992; 38(2): 713-8. https://doi.org/10.1109/18.119732

[49] Rosso OA, Larrondo HA, Martin MT, Plastino A, Fuentes MA. Distinguishing noise from chaos. Phys Rev Lett. 2007; 99(15): 154102. https://doi.org/10.1103/PhysRevLett.99.154102

[50] Wang GJ, Xie C, Stanley HE. Correlation structure and evolution of world stock markets: evidence from pearson and partial correlation-based networks. Comput Econ. 2018; 51(3): 607-35. https://doi.org/10.1007/s10614-016-9627-7

[51] Addor N, Newman AJ, Mizukami N, Clark MP. The CAMELS data set: catchment attributes and meteorology for large-sample studies. Hydrol Earth Syst Sci. 2017; 21(10): 5293-313. https://doi.org/10.5194/hess-21-5293-2017

[52] Kiparsky M, Joyce B, Purkey D, Young C. Potential Impacts of Climate Warming on Water Supply Reliability in the Tuolumne and Merced River Basins, California. PLOS One. 2014; 9(1): e84946. https://doi.org/10.1371/journal.pone.0084946

[53] Fassnacht SR, Records RM. Large snowmelt versus rainfall events in the mountains. J Geophys Res Atmospheres. 2015; 120(6): 2375-81. https://doi.org/10.1002/2014JD022753

[54] Lombard PJ. Flood of April and May 2008 in Northern Maine. Scientific Investigations Report. U.S. Geological Survey; 2010 (cited 2026 Jan 11). Report No.: 2010-5003. Available from: https://pubs.usgs.gov/publication/sir20105003

[55] Monthly Climate/Ocean Indices (Time-Series): NOAA Physical Sciences Laboratory. (cited 2026 Jan 10). Available from: https://psl.noaa.gov/data/timeseries/month/

[56] Nilsson P, Uvo CB, Berndtsson R. Monthly runoff simulation: Comparing and combining conceptual and neural network models. J Hydrol. 2006; 321(1): 344-63. https://doi.org/10.1016/j.jhydrol.2005.08.007

[57] Espeholt L, Agrawal S, Sønderby C, Kumar M, Heek J, Bromberg C, *et al*. Deep learning for twelve hour precipitation forecasts. Nat Commun. 2022; 13(1): 5145. https://doi.org/10.1038/s41467-022-32483-x

[58] Salem FM. Gated RNN: The Gated Recurrent Unit (GRU) RNN. In: Salem FM, Ed. Recurrent Neural Networks: From Simple to Gated Architectures. Cham: Springer International Publishing; 2022 [cited 2026 Jan 10]. p. 85-100. https://doi.org/10.1007/978-3-030-89929-5_5

[59] Greff K, Srivastava RK, Koutník J, Steunebrink BR, Schmidhuber J. LSTM: a search space odyssey. IEEE Trans Neural Netw Learn Syst. 2017; 28(10): 2222-32. https://doi.org/10.1109/TNNLS.2016.2582924

[60] Bengio Y, Simard P, Frasconi P. Learning long-term dependencies with gradient descent is difficult. IEEE Trans Neural Netw. 1994; 5(2): 157-66. https://doi.org/10.1109/72.279181

[61] Eskov VM, Eskov VV, Vochmina YuV, Gorbunov DV, Ilyashenko LK. Shannon entropy in the research on stationary regimes and the evolution of complexity. Mosc Univ Phys Bull. 2017; 72(3): 309-17. https://doi.org/10.3103/S0027134917030067

[62] Kim TK. T test as a parametric statistic. Korean J Anesthesiol. 2015; 68(6): 540-6. https://doi.org/10.4097/kjae.2015.68.6.540

[63] Fang W, Ren K, Liu T, Shang J, Jia S, Jiang X, *et al*. An evaluation of random forest based input variable selection methods for one month ahead streamflow forecasting. Sci Rep. 2024; 14(1): 29766. https://doi.org/10.1038/s41598-024-81502-y

[64] Ren K, Fang W, Qu J, Zhang X, Shi X. Comparison of eight filter-based feature selection methods for monthly streamflow forecasting – Three case studies on CAMELS data sets. J Hydrol. 2020; 586: 124897. https://doi.org/10.1016/j.jhydrol.2020.124897

[65] Fish River at Fort Kent. Last updated: Feb 9, 2026. Available from: https://water.noaa.gov/gauges/01013500?utm

[66] Menoni S. Urban Planning for Disaster Risk Reduction and Climate Change Adaptation: A Review at the Crossroads of Research and Practice. Sustainability. 2025; 17(20): 9092. https://doi.org/10.3390/su17209092

[67] Harrs JA, Reinhart V, Vögt V, Scheib JPP, Tewes T, Pohl T, *et al*. Integration of climate information into urban climate change adaptation: A case study of municipal processes in Constance. Clim Serv. 2024; 35: 100495. https://doi.org/10.1016/j.cliser.2024.100495

[68] Sharifi A, Yamagata Y. Principles and criteria for assessing urban energy resilience: A literature review. Renew Sustain Energy Rev. 2016; 60: 1654-77. https://doi.org/10.1016/j.rser.2016.03.028

[69] Fernandes P, Tomás R, Acuto F, Pascale A, Bahmankhah B, Guarnaccia C, *et al*. Impacts of roundabouts in suburban areas on congestion-specific vehicle speed profiles, pollutant and noise emissions: An empirical analysis. Sustain Cities Soc. 2020; 62: 102386. https://doi.org/10.1016/j.scs.2020.102386

[70] Gray M, Wilmers CC, Reed SE, Merenlender AM. Landscape feature-based permeability models relate to puma occurrence. Landsc Urban Plan. 2016; 147: 50-8. https://doi.org/10.1016/j.landurbplan.2015.11.009

[71] Akan AO, Houghtalen RJ. Urban hydrology, hydraulics, and stormwater quality engineering applications and computer modeling. WILEY; 2003.

[72] Chow VT. Applied Hydrology. Int Assoc Sci Hydrol Bull. 1965; 10(1): 82-3. https://doi.org/10.1080/02626666509493376